applied sciences

MDPI

Article

Shear Resistance Assessment of the Y-Type Perfobond Rib Shear Connector under Repeated Loadings

Sang-Hyo Kim, Oneil Han *, Suro Yoon and Tuguldur Boldoo

School of Civil and Environmental Engineering, Yonsei University, Seoul 03722, Korea; sanghyo@yonsei.ac.kr (S.-H.K.); dbstnfh112@yonsei.ac.kr (S.Y.); tuuguu24@yonsei.ac.kr (T.B.)
* Correspondence: oneilhan@yonsei.ac.kr

Abstract: The steel–concrete composite structures consist of two different material parts, which are connected with reliable shear connectors to enable the combined action of the steel and concrete members. The shear connectors may experience either one-directional repeated cyclic loadings or fully reversed cyclic loadings depending on the structural functions and acting loadings. It is essential for structural engineers to estimate the residual shear strength of the shear connectors after action of repeated loads. The characteristics of deteriorating shear capacities of Y-type perfobond rib shear connectors under repeated loads were investigated to estimate the energy dissipating capacity as well as the residual shear strength after repeated loads. To perform the repeated load experiments four different intensities of repeated loads were selected based on the monotonic push-out tests which were performed with 15 specimens with five different design variables. The selected load levels range from 35% to 65% of the representative ultimate shear strength under the monotonic load. In total, 12 specimens were tested under five different repeated load types which were applied to observe the energy dissipating characteristics under various load intensities. It was found that the dissipated energy per cycle becomes stable and converges with the increasing number of cycles. A design formula to estimate the residual shear strength after the repeated loads was proposed, which is based on the residual shear strength factor and the nominal ultimate shear strength of the fresh Y-type perfobond rib shear connectors. The design residual shear strength was computed from the number of repeated loads and the energy dissipation amount per cycle. The reduction factor for the design residual shear strength was also proposed considering the target reliability level. The various reduction factors for the design residual shear strength were derived based on the probabilistic characteristics of the residual shear strength as well as the energy dissipation due to repeated loads.

Keywords: steel–concrete composite structure; Y-type perfobond rib shear connector; repeated loads; energy dissipation; residual shear strength; reduction factor; target reliability; probabilistic characteristic

check for updates

Citation: Kim, S.-H.; Han, O.; Yoon, S.; Boldoo, T. Shear Resistance Assessment of the Y-Type Perfobond Rib Shear Connector under Repeated Loadings. *Appl. Sci.* **2021**, *11*, 7667. https://doi.org/10.3390/app11167667

Academic Editor: Martin Classen

Received: 13 July 2021
Accepted: 18 August 2021
Published: 20 August 2021

Publisher's Note: MDPI stays neutral with regard to jurisdictional claims in published maps and institutional affiliations.

Copyright: © 2021 by the authors. Licensee MDPI, Basel, Switzerland. This article is an open access article distributed under the terms and conditions of the Creative Commons Attribution (CC BY) license (https://creativecommons.org/licenses/by/4.0/).

1. Introduction

As the steel–concrete composite structures are applied widely to various structures, many studies have been performed to investigate the behaviors of the shear connectors in various design conditions such as shear connector types, material properties, load conditions, etc. The shear connectors between steel and concrete parts may experience either one-directional repeated cyclic loadings or fully reversed cyclic loadings depending on the structural functions and acting loads. Many studies related to the performance of shear connectors under cyclic loads have been conducted. If the shear connectors may experience the cyclic loads during the service life, the shear resistance capacity may deteriorate. Therefore, it is essential that the energy dissipation and residual performance related to cyclic behavior of structures have to be evaluated to secure the target performance of the structures.

Many studies have been performed with different types of shear connectors under different loading types: the fully reversed cyclic loading and one-directional cyclic loading

(repeated loading). Bursi and Gramola [1] conducted monotonic loading tests and fully reversed cyclic loading tests with stud shear connectors to evaluate the hysteretic performance of composite beams. Zandonini and Bursi [2] conducted low cyclic tests depending on the diameters of stud shear connectors. They considered the effects of varying the degree of shear connection to evaluate shear strength and ductility of stud shear connections under low cyclic loads. Nakajima et al. [3] conducted fully reversed cyclic loading tests to evaluate the effects of load condition on the shear strength and fatigue strength of stud shear connections. Maleki and Bagheri [4] analyzed the behavior of shear connections composed of channel shear connectors. Reversed cyclic loading tests and monotonic loading tests were conducted for different types of concrete. Studies by Shariati et al. [5–7] evaluated shear strength reduction and ductility of channel and angle shear connections under fully reversed cyclic loads, compared with design codes, and analyzed the failure modes of shear connections. Kim et al. [8–10] conducted fully reversed cyclic loading tests to evaluate the effect of load condition and transverse rebar size, and to compare the shear connection of stud and Y-type perfobond rib shear connectors. Kim et al. [11] conducted fatigue tests on one-direction of Y-type perfobond rib shear connector, which consider service load intensities. Suzuki et al. analyzed the ultimate shear strength by the fully reversed cyclic loads with studs [12] and perfobond rib shear connectors [13]. They suggested that the ultimate shear strength in cyclic loads might be lower than the estimation suggested by design specifications. Thus, the more detailed evaluation formulae for the ultimate shear strengths were proposed. Kisaku et al. [14] proposed the model to estimate the cyclic response of perfobond rib shear connectors. The unloading–reloading process with push-out specimens was performed, and the model was based on the load–slip relations with empirical data. Wang et al. [15–17] performed repeated and monotonic loading tests to define the shear strength for steel block shear connectors, plate perfobond rib shear connectors with notched holes, and groups of studs. Ramesh et al. [18] tried to define the scope for the use of shear connectors by repeated loading. They dealt with different types of shear connectors such as I, channel, stud, and Z sections.

In the previous studies [8–11], the stubby Y-type perfobond rib shear connectors were tested to be adopted for the steel beam-RC slab composite system in the multi-bay, multi-story frame. The stubby Y-type perfobond rib height is very short and 50 mm high (the total height is 85 mm including the root and dowel hole) to be embedded in the shallow depth RC slab (150 mm deep slab specimens) and the concrete compressive strength is designed to be around 30 MPa. In addition, the cyclic loads are applied to be fully reversed cyclic loadings to simulate the loading conditions during earthquakes. This study investigates the deteriorating shear strength capacities of Y-type perfobond rib shear connectors under the one-directional repeated loadings, in which the rib height is designed to be tall and 100 mm high (the total height is 160 mm including the root and dowel hole) to provide high shear resistances. Therefore, the embedded concrete slab in test specimen is 280 mm deep and the concrete compressive strength is designed to be about 60 MPa. The applied testing loads are designed to be one directional without any reversal loads, which may be experienced in the anchor systems of tension cables. It is planned to suggest how to predict the residual shear strength of the shear connectors after repeated one directional loads. The design formula for the residual shear strength after the repeated loads is proposed based on the probabilistic characteristics of the nominal shear strength as well as the strength degradation with the energy dissipations due to the repeated loads. The residual shear strength formula is proposed according to the target reliability levels. The proposed procedure to generate the design formula of the residual shear strength may be applied to various types of shear connectors under the repeated loads.

2. Details of Monotonic and Repeated Loading Test Program

2.1. Specimen Details

The push-out tests on the specimens with various Y-type perfobond rib shear connectors were conducted to verify the effects of basic design variables, such as rib shape, rebar

diameter, concrete strength, etc., in previous studies [11,19–22]. To extend the application ranges of Y-type perfobond rib shear connectors, the design variables of the additional specimens were selected considering the previously adopted design variables. Table 1 shows the details of the design variables of the specimens in this study. The Y-rib shapes were fixed to have the width of 80 mm, the height of 100 mm, and the thickness of 10 mm. The steel grade was SM490 [23] for all of the specimens. To provide the balanced action between Y-rib and rebar, the rebars were selected from three different diameters in two different rebar grades (SD400 and SD500). SM490 has a nominal yield strength of 315 MPa, and SD400 and SD500 have nominal yield strengths of 400 and 500 MPa, respectively.

Table 1. Design variables of specimens.

Specimen	Number of Specimens (M/R) *	Y-Type Perfobond Rib Shear Connector				Transverse Rebar		Concrete Design Strength (MPa)
		w (mm)	h (mm)	t (mm)	Steel Grade	d_r (mm)	Steel Grade	
SD400-D16-M/R	6 (3/3)	80	100	10	SM490	16	SD400	60
SD400-D19-M/R	6 (3/3)	80	100	10	SM490	19	SD400	60
SD500-D16-M/R	6 (3/3)	80	100	10	SM490	16	SD500	60
SD500-D19-M/R	6 (4/2)	80	100	10	SM490	19	SD500	60
SD500-D22-M/R	3 (2/1)	80	100	10	SM490	22	SD500	60

* w: width; * h: height; * t: thickness; * d_r: diameter of rebar; * respective number of specimens for monotonic (M) and repeated (R) loading tests.

2.2. Fabrication of Specimens and Material Properties

In total, 27 specimens were fabricated for both monotonic and repeated loading tests following the standard specimen form suggested in Eurocode-4 [24]. Figure 1 shows the details of the specimen and Y-type perfobond rib shear connectors. The Y-type perfobond rib shear connectors were welded on the H-beam and embedded in the concrete block. The H-beam has a cross-section of H300 × 300 × 9 × 14 mm, and the concrete block is 600 × 750 × 280 mm.

The fabrication process is shown in Figure 2. All specimens have a 70 mm long styrofoam attached at the bottom end of the Y-type perfobond rib shear connector to remove the end-bearing effect. Additionally, grease was spread on all the interfaces of steel plate and concrete to remove the chemical bond effect before casting the concrete.

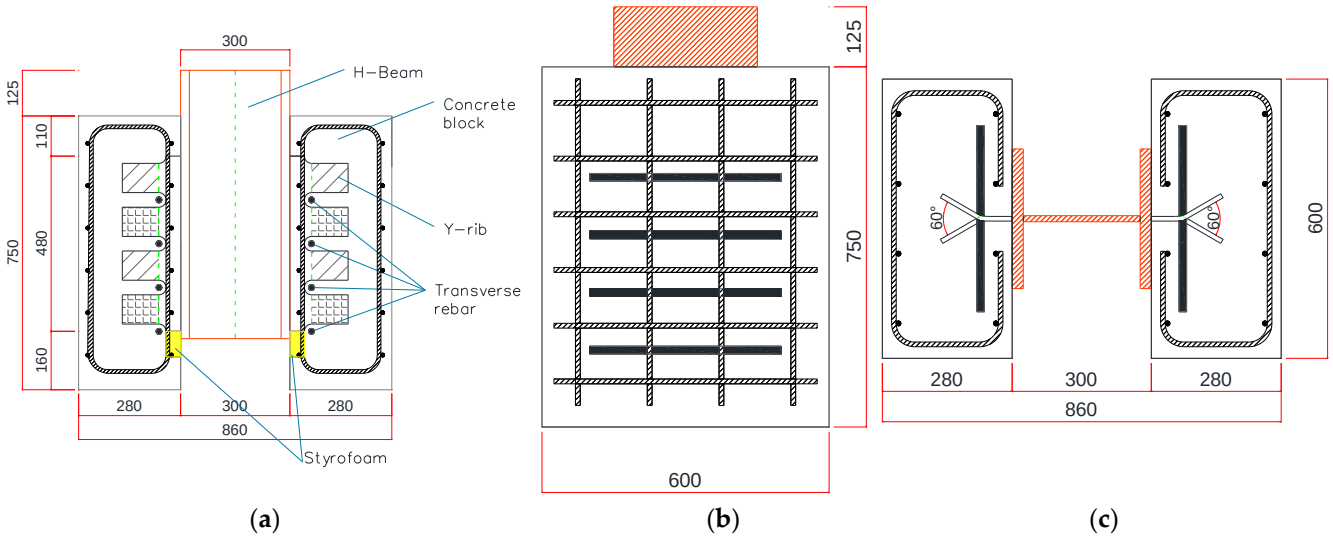

Figure 1. *Cont.*

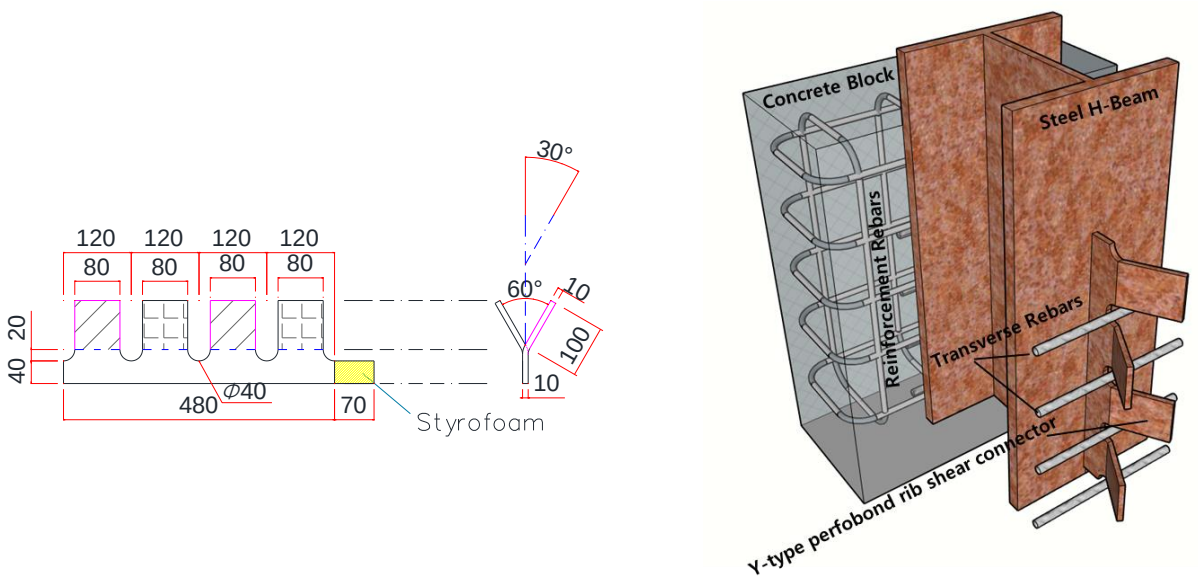

(**d**) (**e**)

Figure 1. Dimensions of the push-out specimen with the Y-type perfobond rib shear connector (unit: mm). (**a**) Front view, (**b**) side view, (**c**) plan view, (**d**) Y-type perfobond rib shear connector and (**e**) push-out specimen with 3D.

The concrete compressive strengths were evaluated through the cylinder tests on both the 28th day and the dates of the monotonic and repeated loading tests. All of the cylinder specimens were cured in the same conditions as the specimens. Table 2 contains the concrete strength data. In this study, 62.4 MPa was adopted as the representative concrete strength.

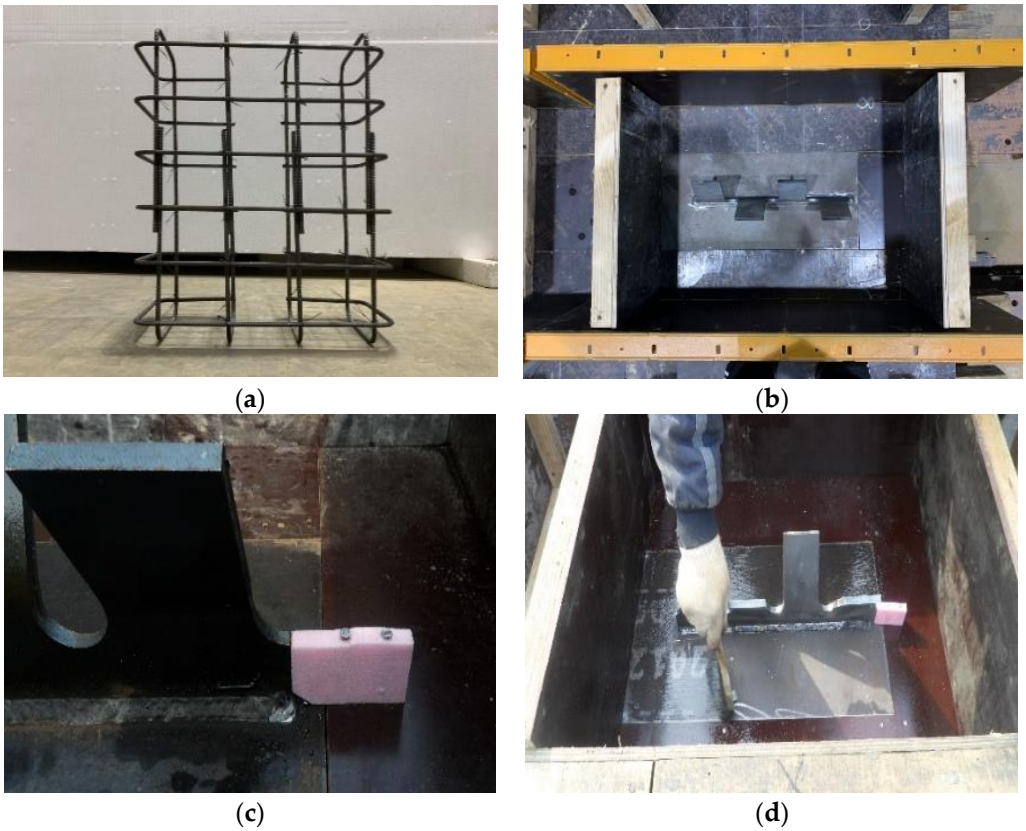

(**a**) (**b**)

(**c**) (**d**)

Figure 2. *Cont.*

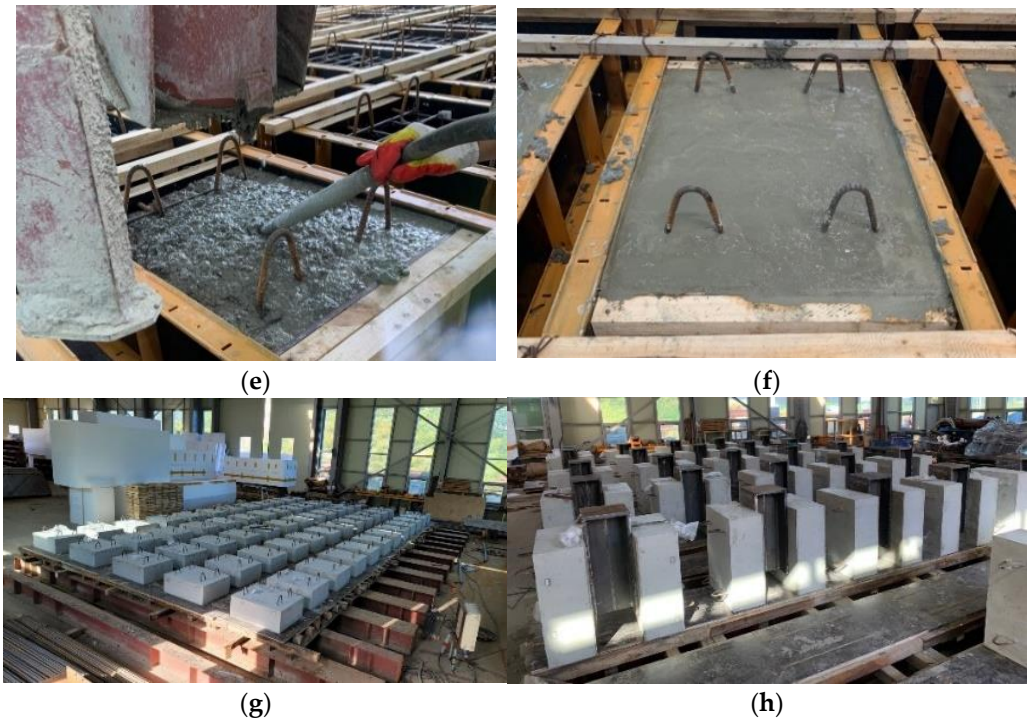

Figure 2. Fabrication process of specimens. (**a**) Rebar mesh, (**b**) formwork, (**c**) styrofoam installation, (**d**) spreading grease, (**e**) concrete pouring, (**f**) concrete compaction, (**g**) removal of forms and (**h**) specimen completed.

Table 2. Concrete compressive strength (unit: MPa).

Type	28-Day		Test Date	
	Remicon #1	Remicon #2	Remicon #1	Remicon #2
Experimental data	62.0, 61.4, 59.7, 61.9, 58.0, 61.5	65.7, 65.6, 63.3, 59.5, 61.9, 64.5, 60.6	63.5, 58.7, 62.8, 63.0, 61.0, 66.1, 63.1, 61.9, 60.8, 62.0	62.8, 64.6, 63.1, 63.5, 63.8, 63.1, 61.5, 61.8, 61.2, 59.8, 62.3, 65.0, 62.6
Mean	60.8	62.9	62.2	62.5
COV	0.013	0.026	0.015	0.019
Avg. strength	61.8		62.4	

The steel plates and rebars were tested through the standard tensile strength tests with steel plate coupons and rebar coupons. As shown in Table 3, all coupons satisfy the Korean Standard [23] in terms of the minimum yield stress (315 MPa) and tensile strength (490 MPa) of SM490, respectively. The minimum yield strengths of SD400 coupons and SD500 coupons are over 400 and 500 MPa, respectively.

Table 3. Material properties for steel plate and reinforcements (unit: MPa).

Type	Number of Specimens	Yield Strength		Tensile Strength	
		Test	Avg.	Test	Avg.
D16 (SD400)	3	461, 461, 468	463.3	585, 587, 584	585.3
D19 (SD400)	3	482, 479, 480	480.3	595, 594, 591	593.3
D16 (SD500)	3	534, 538, 551	541.0	659, 668, 676	667.7
D19 (SD500)	3	550, 547, 543	546.7	674, 673, 670	672.3
D22 (SD500)	3	553, 549, 552	551.3	676, 672, 674	674.0
T10 (SM490)	3	408, 406, 407	407.0	546, 550, 552	549.3

2.3. Strain Gauge Plan

To investigate the yield mechanism of ribs and rebars, the strain gauges were attached to the Y-ribs and transverse rebars and the strains were measured with the applied loading and slip during the application of monotonic load. As listed in Table 4, three specimens were selected to measure the strains in the same manner. Figure 3 shows the strain gauge deployments on the Y-ribs and transverse rebars. The points of measurement were the expected maximum tensile points, which were near the dowel holes in both sides. The measurement points for transverse rebars were the contact points with Y-ribs at the centers of the rebar.

Table 4. Specimens applied with the strain gauge plan.

Specimen	Load Type
SD400-D16-3M	Monotonic load
SD500-D16-3M	Monotonic load
SD500-D19-3M	Monotonic load

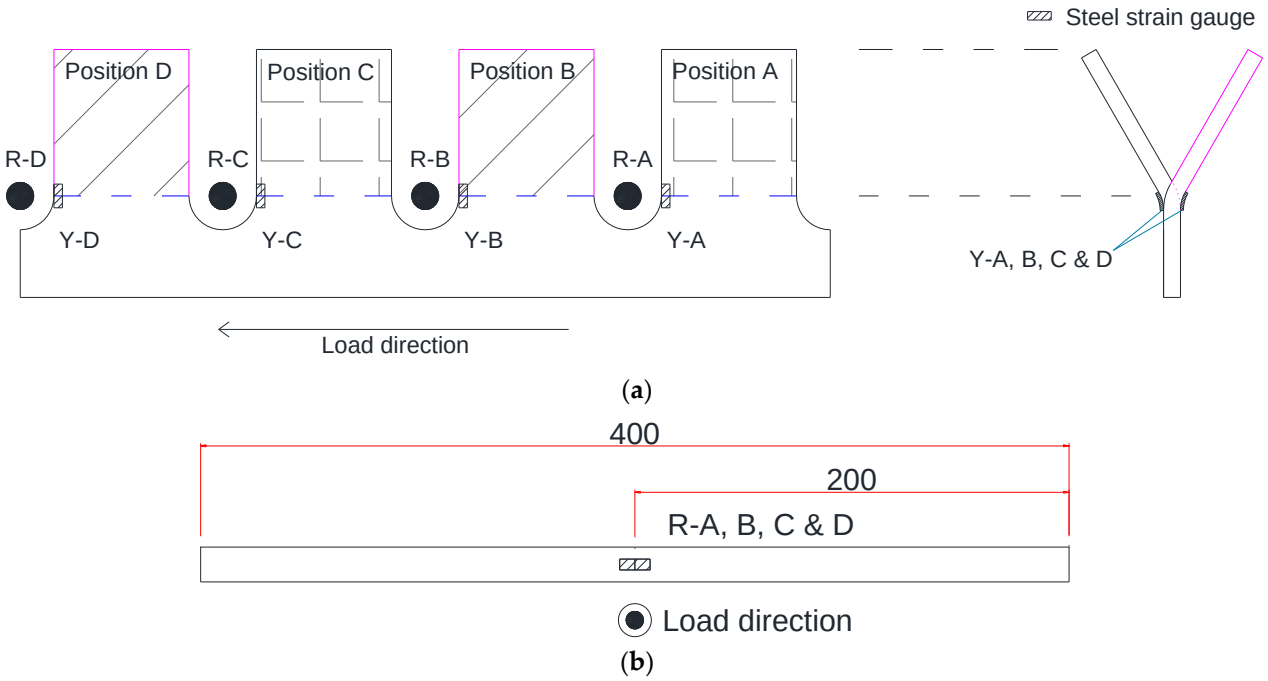

Figure 3. Specifications of points of steel strain gauges. (**a**) Points of steel strain gauges on a Y-rib and (**b**) points of steel strain gauges on a transverse rebar.

3. Monotonic and Repeated Loading Tests

3.1. Monotonic Loading Test

3.1.1. Test Procedure

The monotonic loading tests were performed following the standard push-out test procedures suggested in Eurocode-4 [24]. A universal testing machine (UTM) with a capacity of 3000 kN was used for loading, and the displacement loading rate was set to be 0.05 mm/s. The loading was terminated when the relative displacement exceeded 70 mm. Four LVDTs (Linear Variable Differential Transducers) of 100 mm type, were installed in the middle of the specimen. The relative displacements were averaged from four measurements. Figure 4 shows the test set-up of the push-out tests.

Figure 4. Test set-up of the push-out test.

3.1.2. Shear Resistance and Ductility

The shear resistance and ductility of Y-type perfobond rib shear connectors were evaluated from the monotonic loading test. Figure 5 defines the characteristic values related to the shear resistance and ductility of Y-type perfobond rib shear connectors [19], which are based on Eurocode-4 [24]. The characteristic load (P_{RK}) is defined as the value of 90% of the ultimate shear strength (P_u), which estimates the ultimate slip (δ_u) and characteristic slip (δ_{90}). The characteristic slip (δ_{uk}) is defined as the value of 90% of the ultimate slip (δ_u), which determines the ductile behavior in Eurocode-4 [24]. This study evaluates the ductility with the ratio (δ_u/δ_{90}) based on the characteristic slip (δ_{90}) and ultimate slip (δ_u) suggested by Kim et al. [19].

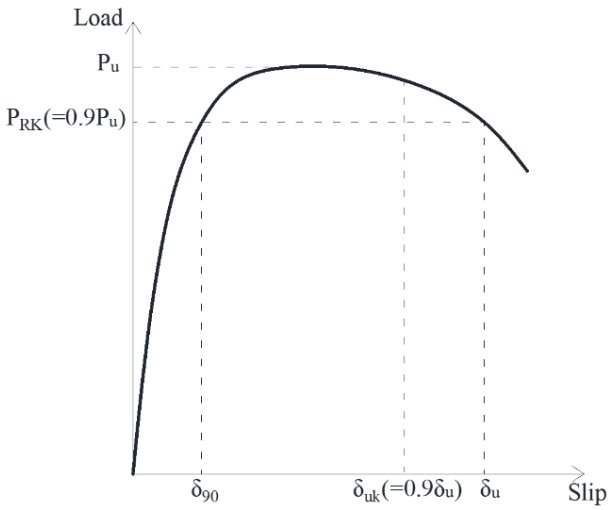

Figure 5. Evaluation method of shear resistance and ductility.

Table 5 summarizes the results of the shear resistance and ductility for all of the specimens, and Figure 6 shows the load–slip curves. It is found that the higher rebar grade does not increase the shear resistance and does not contribute to the ductile behavior. The

specimens with D19 rebars show much higher shear resistances as well as ductility-related slips compared to the specimens with D16 rebars. It is quite important to select the proper size rebars, which may keep balances with the stiffness of Y-ribs. It needs to be noticed that the increasing rate of the shear resistance from D19 specimens to D22 specimens is not much and the ductility-related values are even reduced (δ_u, δ_{uk}, and δ_u/δ_{90}). In Figure 6f, the average load–slip curve for D22 rebars shows a faster drop after the peaks of P_u than that for D19 rebars.

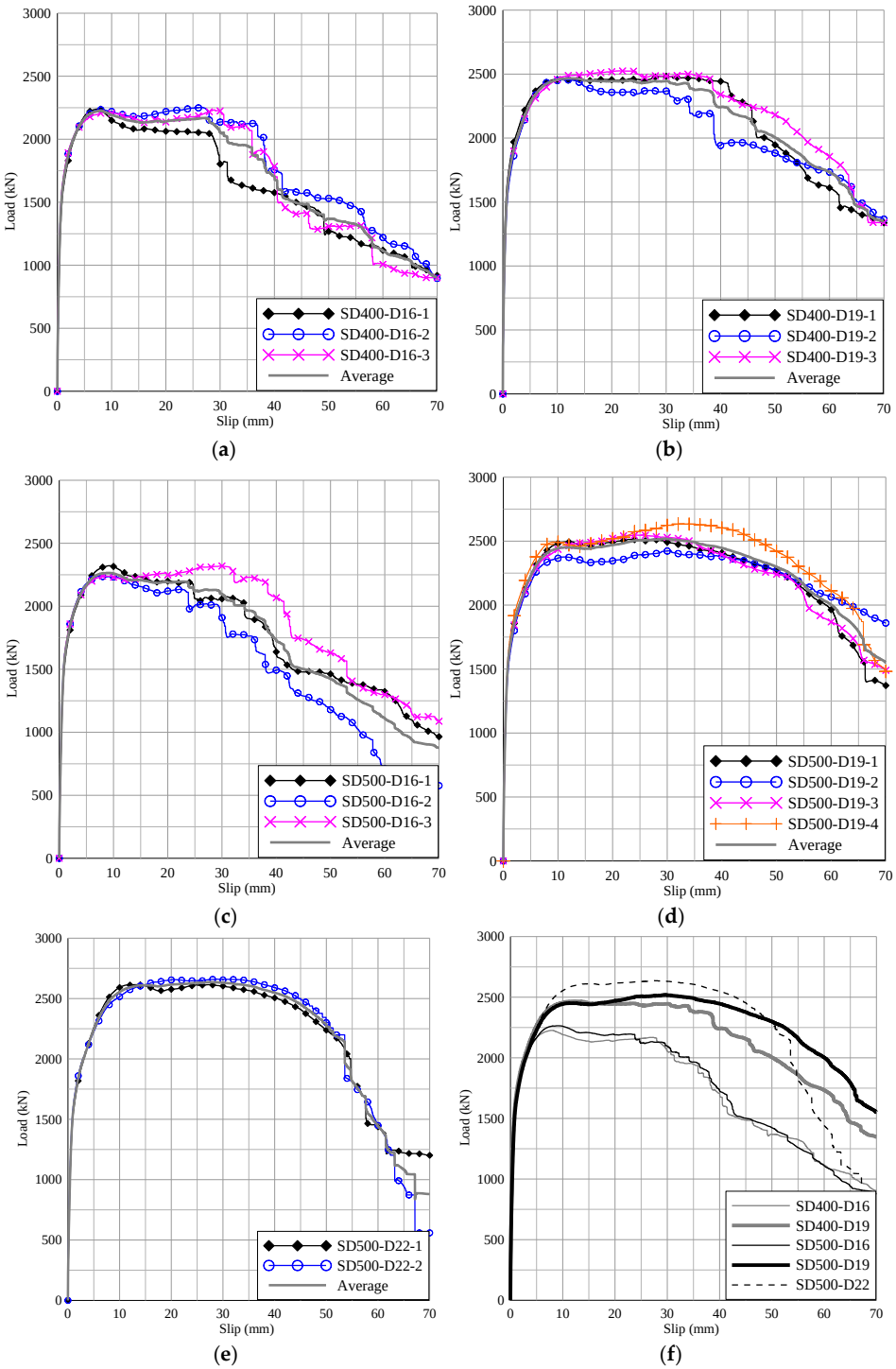

Figure 6. Load–slip curves for monotonic loading tests. (**a**) SD400-D16, (**b**) SD400-D19, (**c**) SD500-D16, (**d**) SD500-D19, (**e**) SD500-D22 and (**f**) averaged load–slip curves.

Table 5. Test results of shear resistance and ductility.

Specimen	No.	P_u (kN)	δ_u (mm)	δ_{uk} (mm)	δ_{90} (mm)	δ_u/δ_{90}
SD400-D16	1 M	2240.3	28.7	25.8	3.2	9.0
	2 M	2234.3	37.5	33.2	4.1	9.2
	3 M	2210.9	35.4	32.0	2.7	13.2
	Avg.	2228.5	33.9	30.4	3.3	10.5
SD400-D19	1 M	2458.0	45.6	41.0	3.9	11.6
	2 M	2456.1	34.2	30.8	4.6	7.5
	3 M	2496.3	45.7	39.0	5.0	9.1
	Avg.	2470.1	41.8	36.9	4.5	9.4
SD500-D16	1 M	2321.1	24.9	22.3	4.0	6.3
	2 M	2240.3	23.8	21.4	3.0	7.9
	3 M	2239.7	41.0	35.1	3.0	13.5
	Avg.	2267.0	29.9	26.3	3.3	9.2
SD500-D19	1 M	2493.2	50.5	45.1	5.1	9.8
	2 M	2547.0	56.1	40.9	4.6	12.3
	3 M	2375.7	45.4	49.0	6.0	7.5
	4 M	2493.7	55.9	46.9	4.4	12.8
	Avg.	2477.4	52.0	45.5	5.0	10.6
SD500-D22	1 M	2614.7	46.7	42.0	5.9	7.9
	2 M	2656.5	47.9	43.2	7.0	6.9
	Avg.	2635.6	47.3	42.6	6.4	7.4

3.1.3. Load–Strain Curve

Based on steel's yield strength, the yield strains for Y-rib and rebar were calculated using Equation (1) [24] and listed in Table 6.

$$\varepsilon_{s,y} = f_{yt} / E_s \quad (1)$$

where $\varepsilon_{s,y}$ is the yield strain, f_{yt} is the yield strength of either Y-rib or rebar (Table 3), and E_s is the Young's modulus (210,000 MPa for both of Y-rib and rebar) [24].

Table 6. Yield strength corresponding to the yield strains for each steel.

Specimen	Y-Rib		Transverse Rebar	
	Yield Strain	Yield Load	Yield Strain	Yield Load
SD400-D16-3M	0.0019	1440.3 kN	0.0022	1556.4 kN
SD500-D16-3M	0.0019	1214.9 kN	0.0023	1567.3 kN
SD500-D19-3M	0.0019	1381.4 kN	0.0026	1757.3 kN
Average	0.0019	1345.5 kN	0.0024	1627.0 kN

The load–strain curves for SD400-D16-3M, SD500-D16-3M, and SD500-D19-3M under the monotonic loadings are plotted in Figure 7. The yield points are plotted in dotted lines in Figure 7 and the yield loads are summarized in Table 6. It is found that the Y-rib yields in advance to the yield of rebar. The intensities of the repeated loads were selected based on the yield load intensities for the Y-ribs.

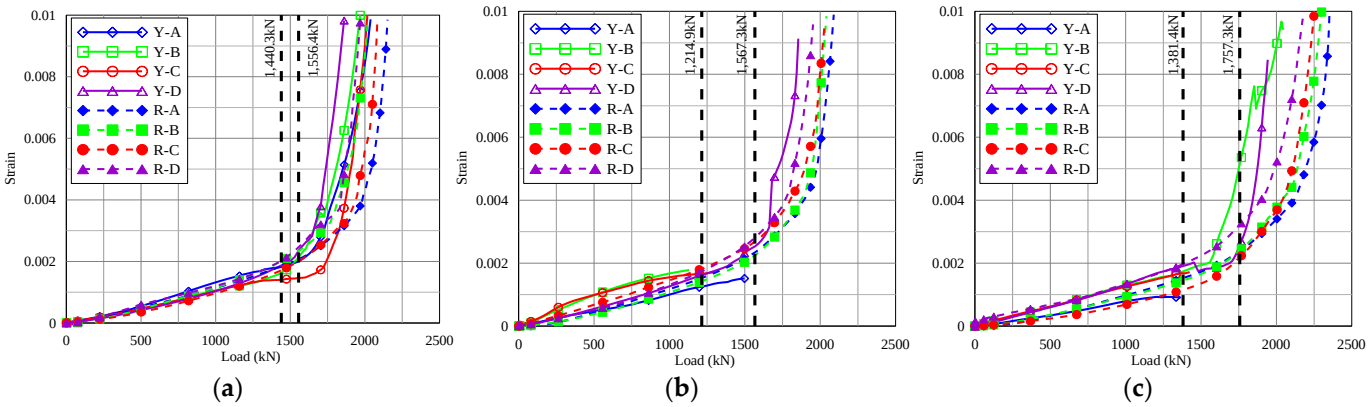

Figure 7. Load–strain curves. (**a**) SD400-D16-3M, (**b**) SD500-D16-3M and (**c**) SD500-D19-3M.

3.2. Repeated Loading Test

3.2.1. Test Procedure

The intensity of repeated loads was based on the Y-rib reaching its yield point earlier than that of the transverse rebar regardless of transverse rebar type. In the initial phase of shear behavior, due to the low effect of transverse rebar types, the same intensity of repeated loads was applied to all of the specimens. Thus, the intensities of repeated loads were determined by the 35%, 45%, 55%, and 65% of the averaged ultimate load of 2245.2 kN (D16, reference ultimate load in Figure 8). The corresponding loads by stage were 785, 1010, 1235, and 1460 kN as listed in Table 7. The maximum allowable load intensity was set to be 1235 kN, because the reference yield load of the Y-rib is 1345.5 kN on average (Table 6). As 1460 kN of applied load is in the range of the two reference loads of 1345.5 (Y-rib yield load) and 1627.0 kN (rebar yield load), it may not be recommended as an allowable load. Using a load over the yield point of the Y-rib was adopted only for the analysis of shear behavior. Figure 8 shows the load–slip curves of the monotonic loading tests and marks the proposed intensities of repeated loads in this study.

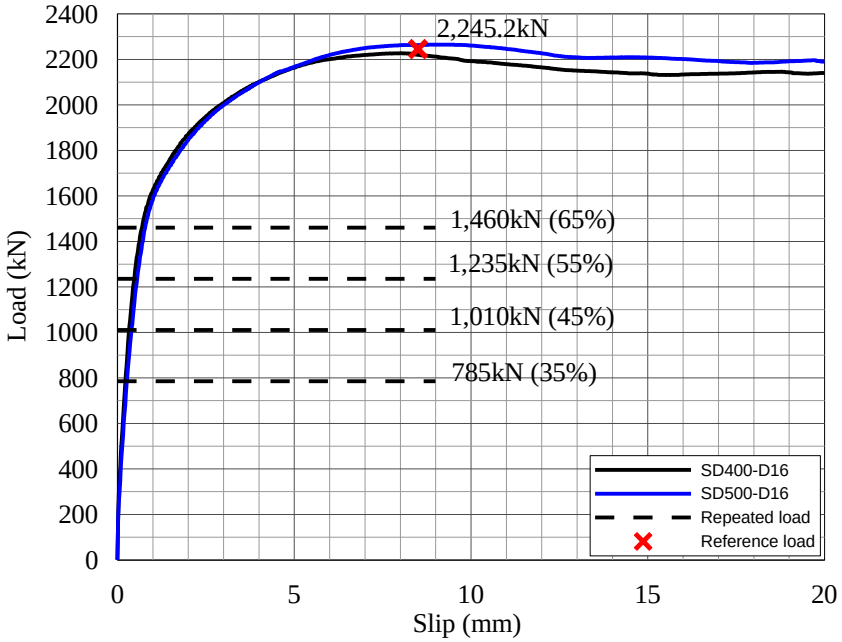

Figure 8. Range of the intensities of repeated loads.

Five types of loads were used for the repeated loading tests as shown in Figure 9. The repeated loading increases gradually through each load stage, and then the monotonic loading was applied to the failure in the last stage. The loading rate was 0.05 mm/s in

displacement control for every load type. The load types 1–3, have four stages for the repeated loads, in which the intensities of the loads are 785, 1010, 1235, and 1460 kN for each stage. The load types 4 and 5 have three stages of the repeated loads, in which the intensities of the loads are 785, 1010, and 1235 kN for each stage. Loads are repeated five times for every stage except the last repeated loading stage. For the last loading stage, the number of repeated loads is varying from 5 to 15 times for the load types 1–3, and 25–50 times for load types 4 and 5. The repeated loading programs are listed in Table 8. The repeated loading tests with 12 specimens were conducted by considering various design variables. The test programs are tabulated in Table 9.

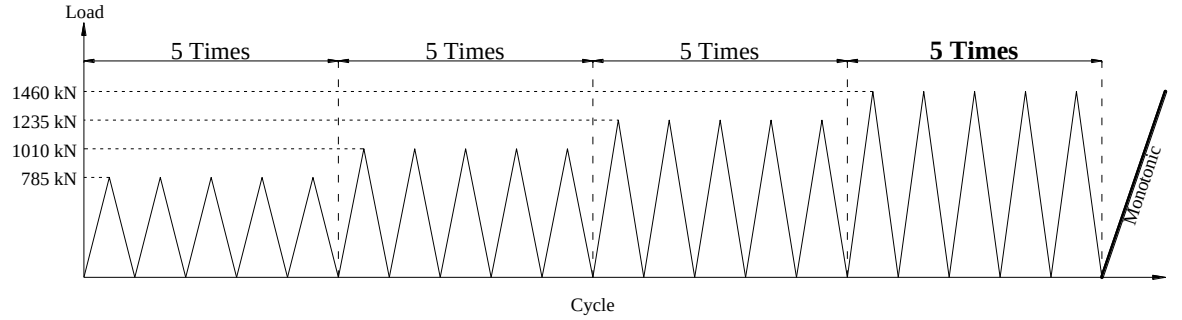

(**a**)

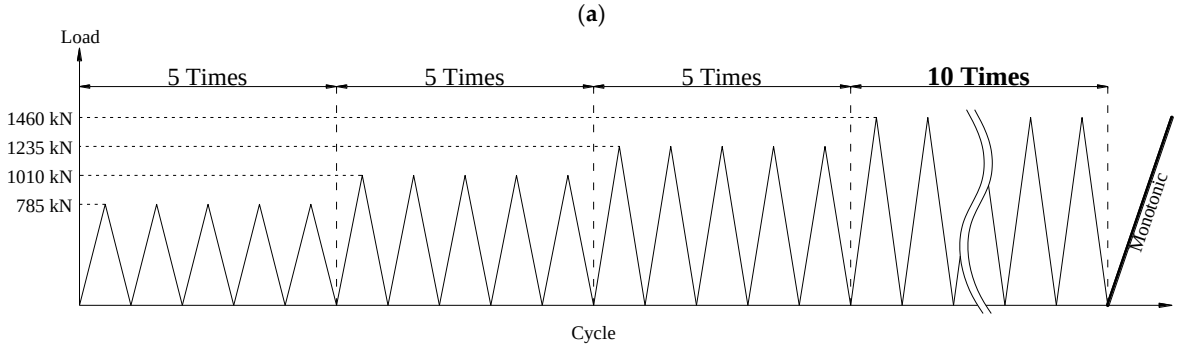

(**b**)

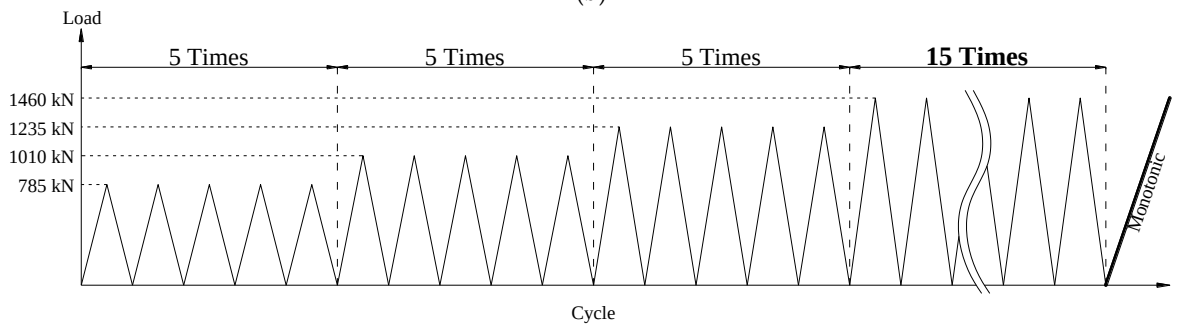

(**c**)

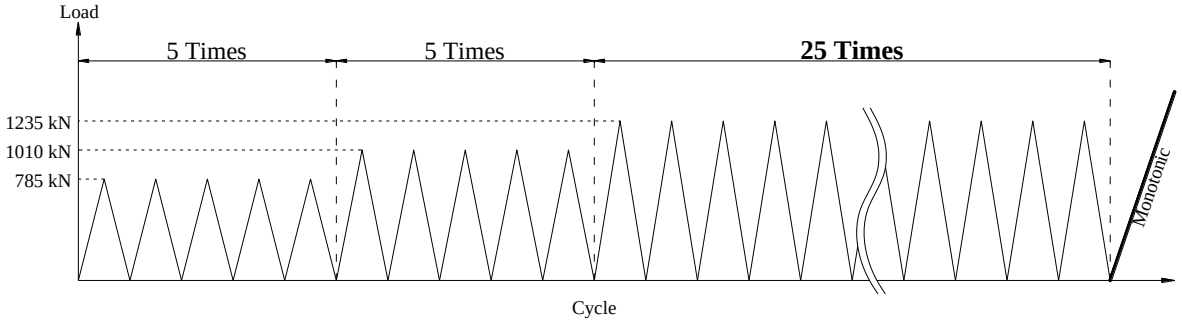

(**d**)

Figure 9. *Cont.*

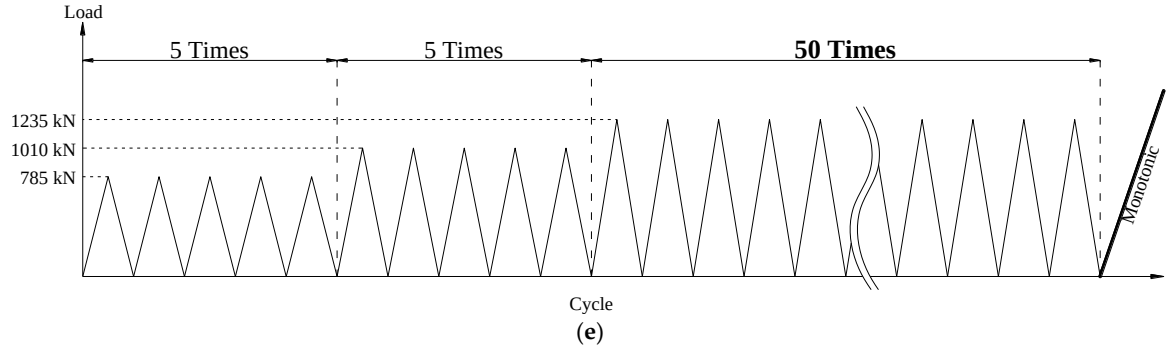

Figure 9. Repeated load types for Y-type perfobond rib shear connectors. (**a**) Load type 1, (**b**) Load type 2, (**c**) Load type 3, (**d**) Load type 4 and (**e**) Load type 5.

Table 7. Intensities of repeated loads for each stage.

Load Stage	Stage 1 (35%)	Stage 2 (45%)	Stage 3 (55%)	Stage 4 (65%)	Stage 5
Intensity	785 kN	1010 kN	1235 kN	1460 kN	Monotonic

Table 8. Repeated loading test programs.

Load Type	Number of Repeated Loads			
	Stage 1	Stage 2	Stage 3	Stage 4
1	5	5	5	5
2	5	5	5	10
3	5	5	5	15
4	5	5	25	-
5	5	5	50	-

Table 9. Repeated loading types for test specimens.

Specimen	Load Type	Specimen	Load Type
SD400-D16-1R	Type 1	SD400-D19-1R	Type 3
SD400-D16-2R	Type 2	SD400-D19-2R	Type 4
SD400-D16-3R	Type 4	SD400-D19-3R	Type 5
SD500-D16-1R	Type 3	SD500-D19-1R	Type 3
SD500-D16-2R	Type 4	SD500-D19-2R	Type 4
SD500-D16-3R	Type 5	SD500-D22-1R	Type 5

3.2.2. Residual Slip Increment under Repeated Loads

The composite Y-type shear connectors may produce residual slips after repeated loads and the increment of residual slip may be related to the deteriorating shear capacity. Figure 10 summarizes the average increments of residual slips due to the repeated load. As shown in Figure 10 the increasing slopes are quite sharp at the beginning stage of experimental load intensities, and the increment per each cycle converges with increasing repeated cycles. However, the repeated load with 1460 kN (65% of ultimate resistance) intensity is found to keep the considerable increment even after 5 cycles (Load Type 2 and 3), whereas the repeated loads with 1235 kN (55%) intensity show the clear convergence in the residual slip increment (Load Type 4 and 5). It can be concluded that the repeated loads with high intensities over 55% of the ultimate shear capacity may not be allowed for the repeated load design with large expected numbers of repetitions.

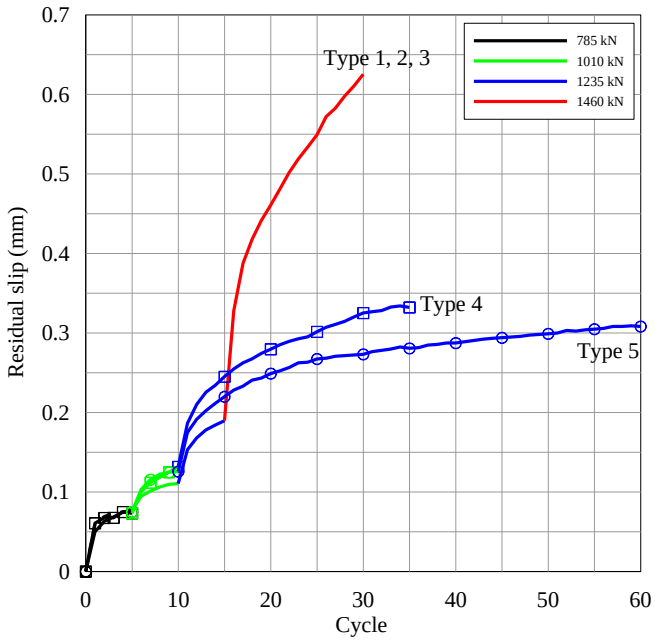

Figure 10. Cumulative residual slip curves according to load cycles.

4. Shear Behavior under Repeated Loads

4.1. Residual Shear Performance after Repeated Loads

4.1.1. Residual Shear Strength

After the Y-type perfobond rib shear connector experiences repeated loads, the ultimate shear strength may decrease. The reduction of shear strength may depend on the repeated number and the intensity of the repeated loads. Table 10 shows the comparisons of the ultimate shear strengths before and after the repeated loads. The reduction ratios of ultimate shear strengths were calculated based on the results of the monotonic loading tests on the fresh specimens without any preceding loadings as well as the specimens loaded with repeated loadings. The reduction ratio depends on the history of the preceding loads. In Table 11, under the load types 1–3, which include 1460 kN loads (65% of the ultimate shear strength), the reduction ratio ranges from 4.1% to 7.1%. However, the reduction ratios are much smaller with the load types 4 and 5, in which the highest load intensity is 1235 kN (55% of the ultimate shear strength). The load types 4 and 5 have minimum 5 times higher numbers of repeats (maximum 30 times). It is concluded that the intensity of repeated loads has a higher effect on the reduction ratio than the number of repeats.

Table 10. Shear resistance degradation by repeated loads.

Specimen (Monotonic)	P_u(A)	Specimen (Repeated)	Load Type	P_u(B)	Ratio (B/A)
SD400-D16	2228.5	SD400-D16-1R	Type 1	2136.4	0.959
		SD400-D16-2R	Type 2	2125.4	0.954
		SD400-D16-3R	Type 4	2188.5	0.982
SD400-D19	2470.1	SD400-D19-1R	Type 3	2309.6	0.935
		SD400-D19-2R	Type 4	2408.9	0.975
		SD400-D19-3R	Type 5	2418.4	0.979
SD500-D16	2267.1	SD500-D16-1R	Type 3	2114.1	0.933
		SD500-D16-2R	Type 4	2224.2	0.981
		SD500-D16-3R	Type 5	2200.5	0.971
SD500-D19	2477.4	SD500-D19-1R	Type 3	2273.6	0.918
		SD500-D19-2R	Type 4	2402.5	0.970
SD500-D22	2635.6	SD500-D22-1R	Type 5	2510.7	0.953

Table 11. Shear resistance degradation by load types.

Load Type	Specimen (Repeated)	Residual Ratio	Averaged Reduction Ratio
Type 1	SD400-D16-1R	0.959	0.041
Type 2	SD400-D16-2R	0.954	0.046
Type 3	SD400-D19-1R SD500-D16-1R SD500-D19-1R	0.935 0.933 0.918	0.071
Type 4	SD400-D16-3R SD400-D19-2R SD500-D16-2R SD500-D19-2R	0.982 0.975 0.981 0.970	0.023
Type 5	SD400-D19-3R SD500-D16-3R SD500-D22-1R	0.979 0.971 0.953	0.031

4.1.2. Residual Ductility

The ductility degradation of the Y-type perfobond rib shear connectors due to the repeated loads was evaluated by comparing with the results of monotonic loading tests. In the both cases, the ductility was evaluated using the method shown in Figure 5. In Table 12, δ_u/δ_{90} after repeated loads do not show noticeable changes. The lowest values of δ_u, δ_{90}, and δ_u/δ_{90} are marked. Even though the lowest values are found from the load types 1–3, in which 1460 kN loads are included, the characteristic values are not much worse than those of the monotonic tests, which are also marked. It is concluded that the ductility deterioration may not be considerable under the repeated loads with the intensity up to 65% of the ultimate shear strength. However, the ductility performance should be examined when the number of repeated loads increases considerably.

Table 12. Characteristic values of displacement ductility according to load conditions.

Monotonic Loading Tests Only				Monotonic Loading Tests after Repeated Loading Tests				
Specimen	δ_u**(mm)**	δ_{90}**(mm)**	δ_u/δ_{90}	**Specimen**	**Load Type**	δ_u**(mm)**	δ_{90}**(mm)**	δ_u/δ_{90}
SD400-D16-1	28.7	3.2	9.0	SD400-D16-1R	Type 1	44.7	2.7	16.5
SD400-D16-2	37.5	4.1	9.2	SD400-D16-2R	Type 2	24.4 *	3.2	7.5
SD400-D16-3	35.4	2.7 *	13.2	SD400-D16-3R	Type 4	24.5	3.5	6.9 *
Average	33.9	3.1	10.5	Average		31.2	3.2	10.3
SD400-D19-1	45.6	3.9	11.6	SD400-D19-1R	Type 3	36.7	5.2	7.0
SD400-D19-2	34.2	4.6	7.5	SD400-D19-2R	Type 4	34.4	4.4	7.9
SD400-D19-3	45.7	5.0	9.1	SD400-D19-3R	Type 5	45.0	4.9	9.2
Average	41.8	4.5	9.4	Average		38.7	4.8	8.0
SD500-D16-1	24.9	4.0	6.3 *	SD500-D16-1R	Type 3	26.8	3.6	7.5
SD500-D16-2	23.8 *	3.0	7.9	SD500-D16-2R	Type 4	39.4	3.7	10.7
SD500-D16-3	41.0	3.0	13.5	SD500-D16-3R	Type 5	33.9	3.5	9.6
Average	29.9	3.3	9.2	Average		33.4	3.6	9.3
SD500-D19-1	50.5	5.1	9.8	SD500-D19-1R	Type 3	25.1	2.0 *	12.9
SD500-D19-2	56.1	4.6	12.3	SD500-D19-2R	Type 4	45.1	5.3	8.5
SD500-D19-3	45.4	6.0	7.5					
SD500-D19-4	55.9	4.4	12.8					
Average	52.0	5.0	10.6	Average		35.1	3.6	10.7
SD500-D22-1	46.7	5.9	7.9	SD500-D22-1R	Type 5	52.5	4.8	10.9
SD500-D22-2	47.9	7.0	6.9					
Average	47.3	6.4	7.4	Average		52.5	4.8	10.9

* Lowest value.

4.2. Energy Dissipation Characteristics under Repeated Loads Depending on Transverse Rebars

The influence of transverse rebar types on energy dissipation under repeated loads was investigated. The energy dissipation per one repeated cycle was calculated as shown in Figure 11. In Figure 11, P1 is the load intensity of the repeated load and δ_1 is the residual slip after the 1st load cycle.

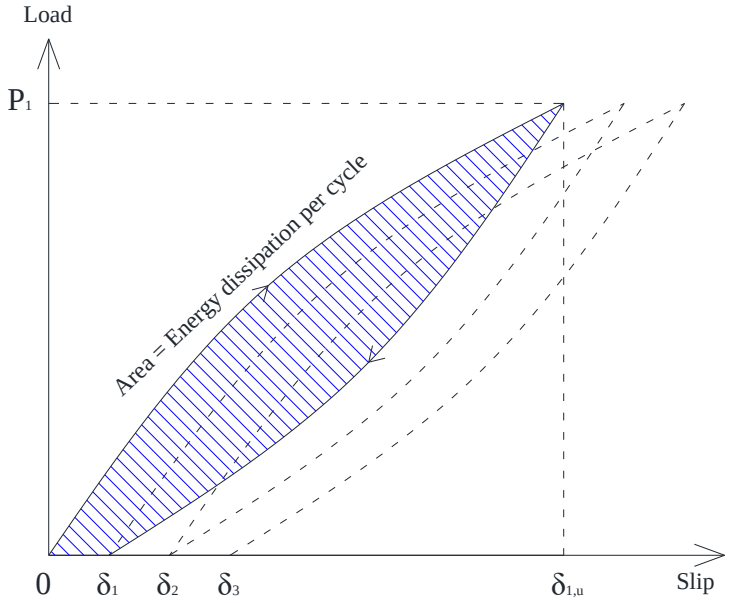

Figure 11. Calculation of energy dissipation per load cycle.

Tables 13–16 summarize energy dissipation amounts under the same loading conditions: Table 13 contains the cumulated energy dissipation due to 5 cycles of repeated loads of 785 kN. Table 14 contains the cumulated energy dissipation due to 5 cycles of repeated loads of 1010 kN after 5 cycles of 785 kN loads are applied in advance. Table 15 summarizes the results of 5-1235 kN loads after 5 cycles of 785 kN and 5 cycles of 1010 kN. Table 16 contains the results of 5-1460 kN loads after 5 cycles of 785 kN, 5 cycles of 1010 kN, and 5 cycles of 1235 kN.

Table 13. Energy dissipation according to transverse rebar type (repeated load = 785 kN) (unit = kN·mm).

Steel Grade	Dia. (mm)	Specimen	Cumulative Energy Dissipation (5 Cycles of 785 kN)	Average 1	Average 2	Average 3
SD400	16	SD400-D16-1R	229.9	249.1	207.7 min: 118.0 max: 277.0	176.4 min: 97.0 max: 277.0
	16	SD400-D16-2R	277.0			
	16	SD400-D16-3R	240.5			
	19	SD400-D16-1R	198.7	166.2		
	19	SD400-D16-2R	118.0			
	19	SD400-D16-3R	181.8			
SD500	16	SD500-D16-1R	183.1	132.0	145.2 min: 97.0 max: 257.0	
	16	SD500-D16-2R	100.9			
	16	SD500-D16-3R	112.0			
	19	SD500-D19-1R	257.0	189.0		
	19	SD500-D19-2R	121.0			
	22	SD500-D22-1R	97.0	97.0		

Table 14. Energy dissipation according to transverse rebar type (repeated load = 1010 kN) (unit = kN·mm).

Steel Grade	Dia. (mm)	Specimen	Cumulative Energy Dissipation (5 Cycles of 1010 kN after 5 Cycles of 785 kN)	Average 1	Average 2	Average 3
SD400	16	SD400-D16-1R	309.9			
	16	SD400-D16-2R	393.4	384.4		
	16	SD400-D16-3R	449.8		308.6	
					min: 180.3	
	19	SD400-D16-1R	277.0		max: 449.8	
	19	SD400-D16-2R	180.3	232.8		267.0
	19	SD400-D16-3R	241.1			min: 158.0
SD500	16	SD500-D16-1R	256.0			max: 449.8
	16	SD500-D16-2R	169.1	204.1		
	16	SD500-D16-3R	187.3		225.4	
					min: 158.0	
	19	SD500-D19-1R	411.5	290.9	max: 411.5	
	19	SD500-D19-2R	170.2			
	22	SD500-D22-1R	158.0	158.0		

Table 15. Energy dissipation according to transverse rebar type (repeated load = 1235 kN) (unit = kN·mm).

Steel Grade	Dia. (mm)	Specimen	Cumulative Energy Dissipation (5 Cycles of 1235 kN after 5 Cycles of 785 kN–5 Cycles of 1010 kN)	Average 1	Average 2	Average 3
SD400	16	SD400-D16-1R	536.5			
	16	SD400-D16-2R	571.6	641.4		
	16	SD400-D16-3R	816.0		518.7	
					min: 324.9	
	19	SD400-D16-1R	445.9		max: 816.0	
	19	SD400-D16-2R	324.9	396.1		463.1
	19	SD400-D16-3R	417.4			min: 310.2
SD500	16	SD500-D16-1R	472.7			max: 816.0
	16	SD500-D16-2R	310.4	379.2		
	16	SD500-D16-3R	354.6		407.5	
					min: 310.2	
	19	SD500-D19-1R	648.2	479.2	max: 648.2	
	19	SD500-D19-2R	310.2			
	22	SD500-D22-1R	348.7	348.7		

Table 16. Energy dissipation according to transverse rebar type (repeated load = 1460 kN) (unit = kN·mm).

Steel Grade	Dia. (mm)	Specimen	Cumulative Energy Dissipation (5 Cycles of 1460 kN after 5 Cycles of 785 kN–5 Cycles of 1010 kN–5 Cycles of 1235 kN)	Average 1	Average 2	Average 3
SD400	16	SD400-D16-1R	1061.2			
	16	SD400-D16-2R	940.4	1000.8		
	16	SD400-D16-3R	-		958.6	
					min: 874.1	
	19	SD400-D16-1R	874.1		max: 1061.2	
	19	SD400-D16-2R	-	874.1		977.3
	19	SD400-D16-3R	-			min: 874.1
SD500	16	SD500-D16-1R	930.0			max: 1080.5
	16	SD500-D16-2R	-	930.0		
	16	SD500-D16-3R	-		1005.3	
					min: 930.0	
	19	SD500-D19-1R	1080.5	1080.5	max: 1080.5	
	19	SD500-D19-2R	310.2			
	22	SD500-D22-1R	348.7	348.7		

It is found that the energy dissipation amounts do not show the dependency on the rebar diameters (D16, D19, D22) as well as the rebar materials (SD400, SD500) as long as the Y-type perfobond rib shear connectors are loaded repeatedly with the intensities below 65% of the ultimate shear resistance. As mentioned with the results of load–strain measurements, the transverse rebars do not exceed the yield strains up to the load level

of 65% of the ultimate shear resistance. It can be concluded that the energy dissipation models may be generated only depending on the load intensities of the repeated loads for the specimens adopted in this study.

5. Residual Shear Strength Design Procedure under Repeated Loads

5.1. Energy Dissipation Models under Repeated Loads

The energy dissipations per one repeated load cycle are summarized in Tables A1–A4 depending on the load intensities from 785 to 1460 kN. For the relatively low intensities, such as 785 and 1010 kN, the average values of energy dissipations per cycle converge reasonably after 3 cycles of repeated loads, even though the variation of the energy dissipations for 12 specimens is quite large: from 10 to 50 kN·mm for 785 kN loads (35% of ultimate shear strength) and from 20 to 90 kN·mm for 1010 kN loads (45% of ultimate shear strength). For the repeated load of 1235 kN (55% of ultimate shear strength) the average energy dissipation converges after 10 cycles as shown in Table A3, in which some specimens are loaded repeatedly up to 50 times. For the repeated load of 1460 kN (65% of ultimate shear strength) the average energy dissipation converges also after 9 cycles as shown in Table A4, in which some specimens are loaded repeatedly up to 15 times. The difference of energy dissipation continues to decrease slightly with increasing cycles after the convergence is achieved. This part will contribute to the conservative estimation of total energy dissipation due to the repeated loads during the service life of the structure in the design stage.

To establish the energy dissipation models per one repeated load cycle, 24 energy dissipation results from the 4th and 5th cycles were selected for the sample sets of 785 and 1010 kN loads, respectively. For the 1235 kN load sample set, 24 energy dissipation data were collected from the 10th to 13th cycles, that is, 6 data from each cycle as shown in Table A3. For the energy dissipation model of 1460 kN load, 23 data were collected from the 9th to 15th cycles to generate the sample set as shown in Table A4.

Due to the limited number of specimens, the repeated loading tests with the load types 4 and 5, were performed with selected specimens, that is, 7 specimens out of 12 specimens continue to be tested after 5 cycles of 1235 kN load as shown in Table A3. The other 5 specimens were tested under different loading types (load types 1–3). Based on this, the energy dissipation trends are investigated in Figure 12. The selected 6 specimens for more than 5 cycles of 1235 kN load test (the solid-lined box, 1235-L in Figure 12) show relatively low energy dissipations during the 1010 kN loads (1010-L1 group in Figure 12) compared to the other 6 specimens, which continue to be loaded with 1460 kN after 5 cycles of 1235 kN load. In Table 17, the order of energy dissipating amounts is provided from ①–⑫ for 785 and 1010 kN loads in the increasing order, and ①–⑦ for 1235 kN load, and ①–④ for 1460 kN load. In 785 and 1010 kN columns of Table 17, two averages are provided: one is the average of 12 specimens and the other is the average of 6 selected specimens, which are loaded with 1235 kN repeated loads after 1010 kN repeated loads. One specimen is excluded: No.10 specimen, that is ordered with ⑦ in 1235 kN column, because the energy dissipation amount of No.10 specimen is quite large compared to the other 6 samples. The trend is similar in 785 and 1010 kN. For the 1010 kN loads, the average of the selected 6 specimens (①–⑥ in 1010 kN column) is only 25.99 kN·mm (Average-2), and much lower than the average of whole sample, 45.44 kN·mm (Average-1). Under the repeated loads of 785 kN, two groups of specimens show a very similar trend. Therefore, the expected average of 1235 kN loads may be much larger than 51.07 kN·mm, which is obtained from the selected 6 specimens. Based on this, the ratios of the mean values of 785 and 1010 kN loads were utilized to revise the average value of 1235 kN load. To establish the energy dissipation model for 1460 kN load, the average energy dissipation values of No.6 and No.9 specimens were selected as the representative mean value. The average energy dissipation amount of No.6 and No.9 specimens under 1010 kN loads is 46.50 kN·mm, that is almost same as the average (45.44 kN·mm) of the whole 12 data set.

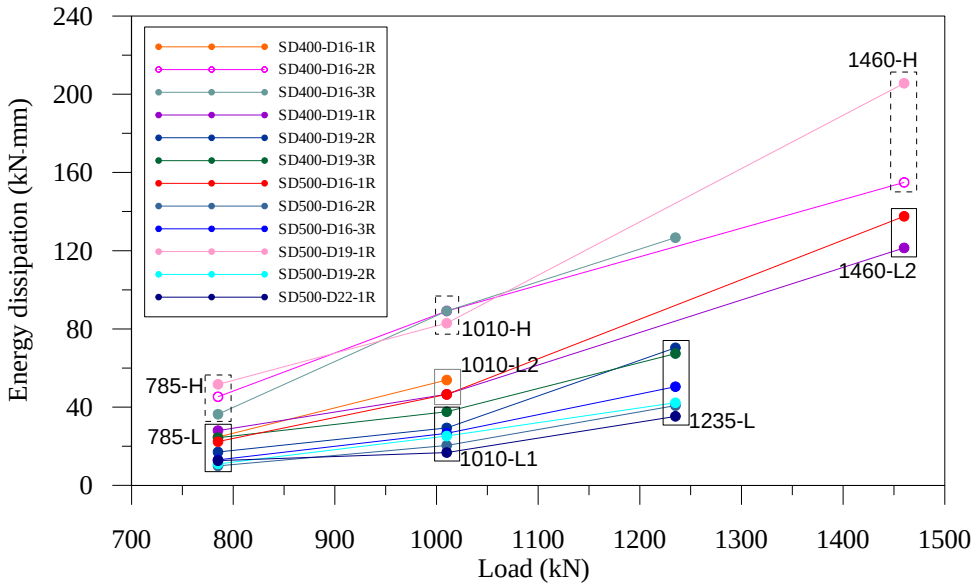

Figure 12. Energy dissipation changes by repeated loads.

Table 17. Energy dissipation on average by specimen.

No.	Specimen	785 kN	1010 kN	1235 kN	1460 kN
1	SD500-D16-2R (Type4)	9.93 ①	20.42 ②	40.77 ②	-
2	SD500-D19-2R (Type4)	10.97 ②	25.19 ③	42.20 ③	-
3	SD500-D22-1R (Type5)	12.60 ③	16.75 ①	35.29 ①	-
4	SD500-D16-3R (Type5)	12.96 ④	26.58 ④	50.43 ④	-
5	SD400-D19-2R (Type4)	17.01 ⑤	29.38 ⑤	70.31 ⑥	-
6	SD500-D16-1R (Type3)	22.32 ⑥	46.47 ⑦	-	137.58 ②
7	SD400-D19-3R (Type5)	24.30 ⑦	37.63 ⑥	67.40 ⑤	-
8	SD400-D16-1R (Type1)	24.72 ⑧	53.82 ⑨	-	-
9	SD400-D19-1R (Type3)	27.99 ⑨	46.54 ⑧	-	121.40 ①
10	SD400-D16-3R (Type4)	36.35 ⑩	89.16 ⑫	126.64 ⑦	-
11	SD400-D16-2R (Type2)	45.28 ⑪	70.47 ⑩	-	154.91 ③
12	SD500-D19-1R (Type3)	51.65 ⑫	82.89 ⑪	-	205.63 ④
Average-1 (All specimens) (A)		24.67	45.44		-
Average-2 (No. 1, 2, 3, 4, 5, 7) (B)		14.63	25.99	51.07 *	-
Ratio of mean value (B/A)		0.59	0.57		-

* Revised.

The probabilistic characteristics of energy dissipations per cycle were investigated with the whole data sets of 785 and 1010 kN. The probability paper fitness tests were performed with various PDFs as summarized in Table 18. The lognormal PDFs are found to provide the best fitness in both 785 and 1010 kN models as shown in Figure 13. The probability models for 1235 kN load and 1469 kN load were artificially revised. Table 19 provides the probabilistic models of the energy dissipations per one repeated load cycle to be applied for the following procedure to estimate the residual shear strength under the repeated loads.

Table 18. Probabilistic characteristics for 785 kN model and 1010 kN model.

Type	PDF	Mean	COV	Correlation Coefficient
785 kN	Normal	24.67	0.586	0.966
	Log-normal	25.89	0.696	0.992 *
	Type-I	25.25	0.612	0.988
1010 kN	Normal	45.44	0.563	0.964
	Log-normal	47.44	0.666	0.985 *
	Type-I	46.45	0.584	0.979

* Best fit.

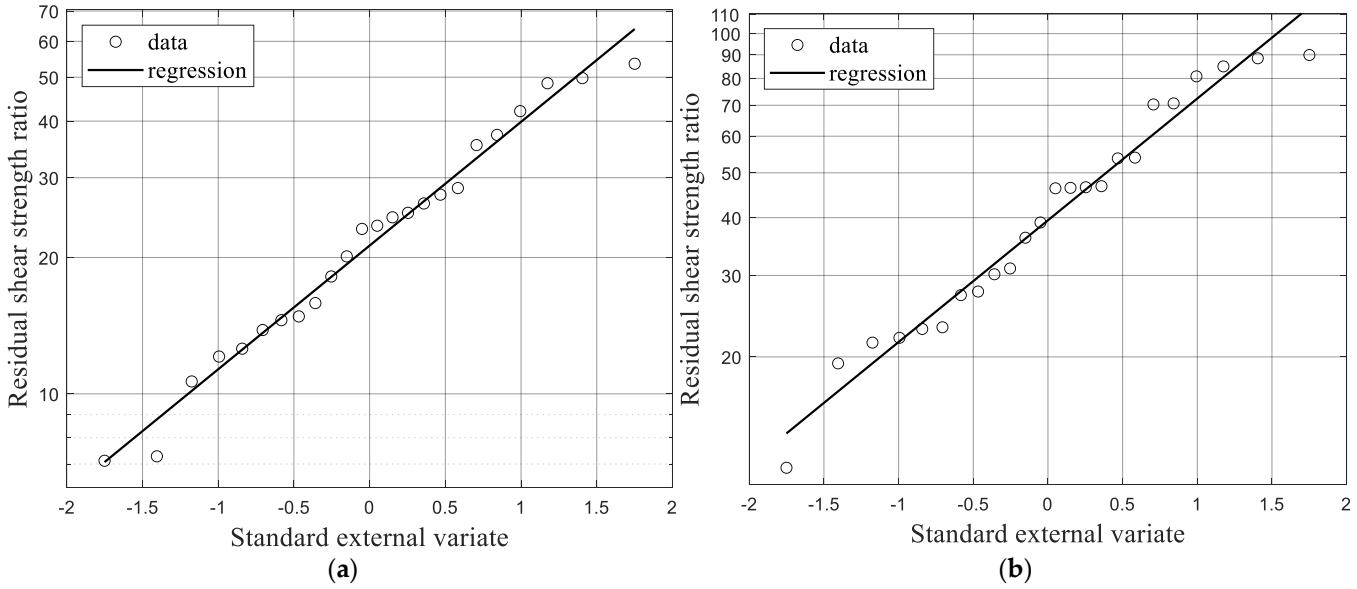

Figure 13. Cyclic energy dissipations on the log-normal probability paper. (**a**) 785 and (**b**) 1010 kN.

Table 19. Probabilistic models of energy dissipation per repeated load.

Load (kN)	Mean (kN·mm)	COV	Distribution
785	25.89	0.696	Log-normal
1010	47.44	0.666	Log-normal
1235	92.85 *	0.636 *	Log-normal
1460	129.49 *	0.606 *	Log-normal

* Revised.

5.2. Design Residual Shear Strength under the Repeated Loads Based on the Actual Shear Strength

5.2.1. Residual Shear Strength Due to the Repeated Loads

The residual shear strength may decrease with repeated loads and is expected to have a relation with the total cumulated energy dissipation. Table 20 summarizes the total energy dissipations with the residual shear strengths. The experimental results are plotted in Figure 14 and it is found that the relation of the residual shear strength and total energy dissipation shows a linear decreasing except two specimens (SD400-D16-3R, SD400-D19-3R in the bold dashed circle), which are found to reserve high residual shear strengths even after high energy dissipations. The reliability of steel–concrete composite structure can be affected by the casting conditions, materials, etc. Therefore, the exception of the two results in the regression process to evaluate the reduction trend of the residual shear strength may contribute as a conservative part.

Based on the regression analysis in Figure 14, the following Equation (2) is proposed as a nominal residual strength factor after repeated loads ($\gamma_{r,E,n}$) for Y-type perfobond rib shear connectors:

$$\gamma_{r,E,n} = 1.00 - 2 \times 10^{-5} n_L E \quad (2)$$

where $\gamma_{r,E,n}$ is the nominal residual strength factor after repeated loads, n_L is the number of repeated loads, and E is the dissipated energy per 1 cycle of repeated load, which should be adopted tentatively from the mean values in Table 19 depending on the intensity of repeated loads.

Therefore, the nominal residual shear strength ($P_{u,r,n}$) (Equation (3)) is calculated from both the nominal residual strength factor (Equation (2)) and the nominal ultimate shear strength (Equation (4)) [25]:

$$P_{u,r,n} = \gamma_{r,E,n} P_{u,n} \quad (3)$$

in which

$$P_{u,n} = {n_r}^{0.67}\left(970 d_r {f_{yr}}^{0.2} + 4240\sqrt{f_y}\left(\frac{t}{10}\right)\left(\frac{w}{80}\right)^{0.95}\left(\frac{h}{100}\right)^{0.45}\right){f_{ck}}^{0.3} \quad (4)$$

where $P_{u,r,n}$ is the nominal residual shear strength, $\gamma_{r,E,n}$ is the nominal residual strength factor, $P_{u,n}$ is the nominal shear strength, n_r is the number of Y-ribs, d_r is the diameter of the transverse rebars, f_{yr} is the yield strength of the transverse rebars, f_y is the yield strength of the Y-ribs, t, w, h are the thickness, width, and height of the Y-ribs, respectively, and f_{ck} is the concrete compressive strength.

Table 20. Comparison of dissipated energy and residual shear strength.

Load Type	Specimen	Total Energy Dissipation (kN·mm)	Residual Shear Strength (A)	Nominal Residual Shear Strength on Regression Line (B)	Ratio (A/B)	Note
1	SD400-D16-1R	2137.6	0.959	0.963	1.001	
2	SD400-D16-2R	3000.3	0.954	0.946	1.015	
3	SD500-D16-1R	3231.0	0.933	0.941	0.997	
	SD400-D19-1R	3031.5	0.935	0.945	0.995	
	SD500-D19-1R	4481.5	0.917	0.916	1.008	
4	SD400-D16-3R	4061.6	0.982	0.977	-	Excluded
	SD500-D16-2R	1444.0	0.981	0.969	1.010	
	SD400-D19-2R	1848.1	0.975	0.977	1.013	
	SD500-D19-2R	1423.9	0.970	0.949	0.998	
5	SD500-D16-3R	2819.6	0.971	0.957	1.029	
	SD400-D19-3R	3882.8	0.979	0.963	-	Excluded
	SD500-D22-1R	2423.1	0.953	0.946	1.001	

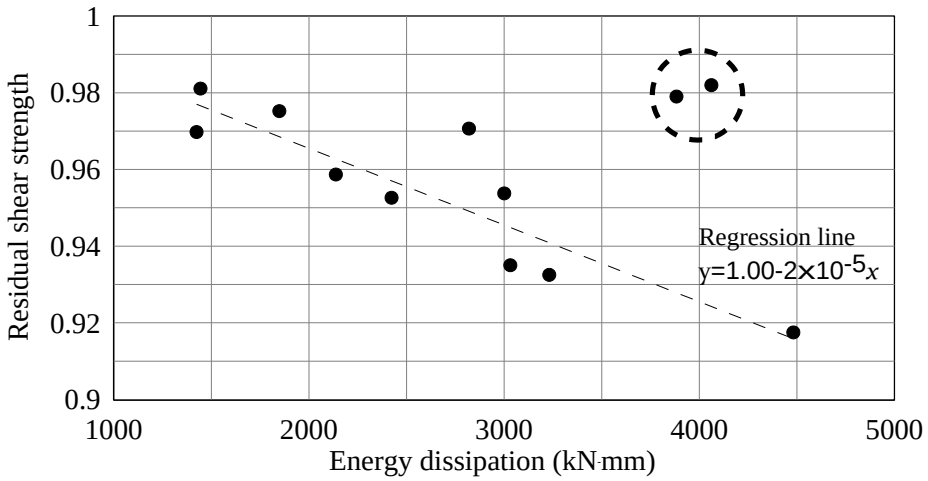

Figure 14. Distribution of residual shear strength and energy dissipation.

The probabilistic characteristics of the residual shear strength ($P_{u,r}$) were investigated with the probabilistic characteristics of the residual shear strength factor and the ultimate shear strength. The variation of the residual shear strength from the nominal value was treated as a bias factor (B_γ) from the nominal residual strength factor ($\gamma_{r,E,n}$) and the bias factors were plotted on various probability papers referred to in Ang et al. [25] as shown in Figure 15. The probabilistic models of bias factors are summarized in Table 21 and the Type-I Gumbel distribution was selected.

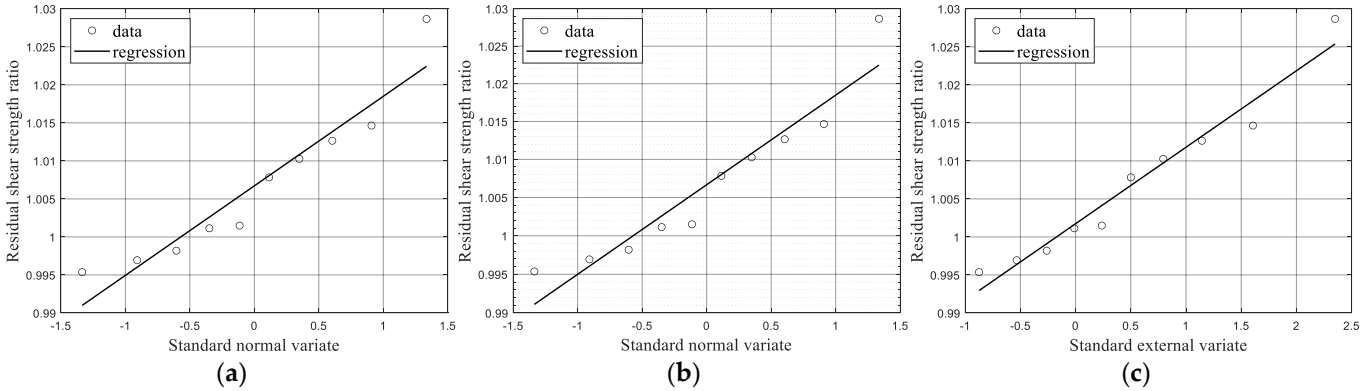

Figure 15. Bias factors of the nominal residual shear strength factor on PDF probability paper. (**a**) Normal, (**b**) Log-normal and (**c**) Type-I.

Table 21. Bias factor (B_γ) models of nominal residual strength factor.

Type	PDF	Mean	COV	Correlation Coefficient
Residual shear strength	Normal	1.0067	0.0117	0.9529
	Log-normal	1.0067	0.0117	0.9542
	Type-I	1.0075	0.0128	0.9802

The probabilistic characteristics of the ultimate shear strength of the fresh shear connectors without any preceding loads (P_u) suggested by Kim et al. [26]:

$$P_u = B_{Pu} P_{u,n} \tag{5}$$

where P_u is the ultimate shear strength, B_{Pu} is the bias factor of the shear strength.

The mean value of the bias factor for the shear resistance formula (P_u) was found to be 1.129 and COV was 0.127, as shown in Table 22 [26]. The probabilistic characteristics of the residual shear strength due to the repeated loads ($P_{u,r}$) were calculated by Monte-Carlo simulation by combining the bias factors of the shear strength and probabilistic characteristics of the residual shear strength. Table 23 shows the results by the number of repeated loads (n_L) with 25, 50, and 100 times. Figure 16 shows the simulation results plotted on the normal papers and it is found that the fitness does not match well to the normal PDF when the total energy dissipation amount becomes large.

Table 22. Bias factor for the shear resistance formula (P_u) [26].

Case	PDF	Mean	COV
4-rib	Normal	1.129	0.127

Table 23. Residual shear strength (normalized) after the repeated loads ($P_{u,r}$).

Number of Repeated Loads (n_L)	Type	785 kN	1010 kN	1235 kN	1460 kN
25	Mean	1.123	1.111	1.084	1.064
	COV	0.128	0.129	0.131	0.135
50	Mean	1.108	1.084	1.031	0.990
	COV	0.129	0.132	0.144	0.156
100	Mean	1.030	0.924	0.843	1.030
	COV	0.146	0.193	0.243	0.146

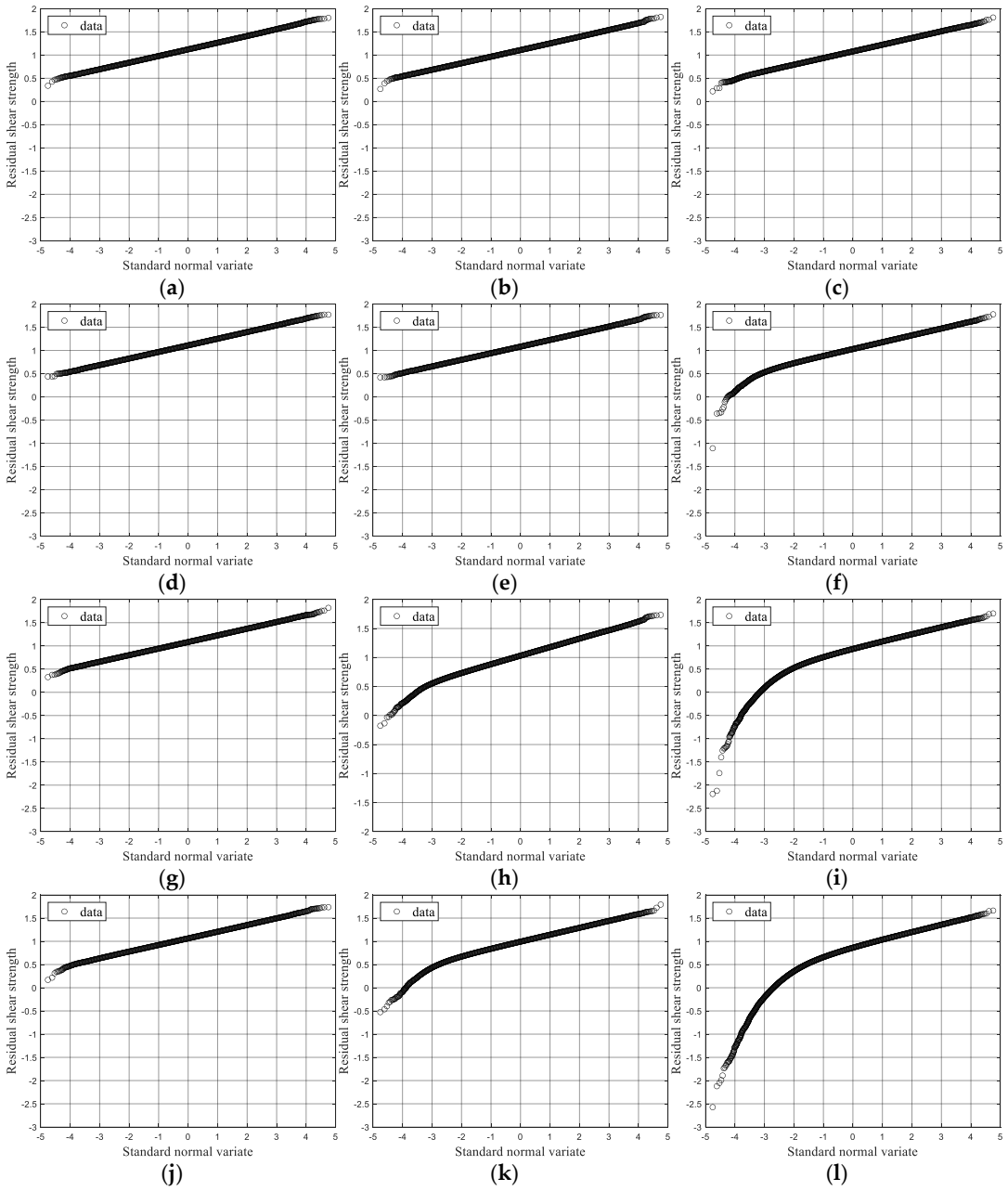

Figure 16. Residual shear strength due to the repeated loads ($P_{u,r}$) on PDF probability paper. (**a**) 785 kN—25 times; (**b**) 785 kN—50 times; (**c**) 785 kN—100 times; (**d**) 1010 kN—25 times; (**e**) 1010 kN—50 times; (**f**) 1010 kN—100 times; (**g**) 1235 kN—25 times; (**h**) 1235 kN—50 times; (**i**) 1235 kN—100 times; (**j**) 1460 kN—25 times; (**k**) 1460 kN—50 times; (**l**) 1460 kN—100 times.

5.2.2. Design Residual Shear Strength under Repeated Loads

The design residual shear strength ($P_{u,r,d}$) is proposed by adopting the reduction factor (ϕ_r) as in Equation (6), in which the reduction factor (ϕ_r) for design residual shear strength to the nominal residual shear strength ($P_{u,r,n}$) depends on the target reliability:

$$P_{u,r,d} = \phi_r P_{u,r,n} \tag{6}$$

where $P_{u,r,d}$ is the design residual shear strength, ϕ_r is the reduction factor for design residual shear strength and $P_{u,r,n}$ is the nominal residual shear strength.

Table 24 contains the various reduction factors (ϕ_r) for design residual shear strength. The reduction factors were selected from the plots in Figure 16 depending on the target

reliability levels (β). The reduction factor (ϕ_r) is listed by the number of repeated loads (n_L), the target reliability levels, and the intensity of repeated loads. The design residual shear strength ($P_{u,r,d}$) can be calculated by combining the reduction factors (ϕ_r) and nominal residual shear strength ($P_{u,r,n}$), which is considered with various design variables.

Table 24. Reduction factor for design residual shear strength (ϕ_r).

Number of Repeated Loads (n_L)	β	785 kN	1010 kN	1235 kN	1460 kN
25	2.0	0.846	0.845	0.838	0.832
	2.5	0.773	0.772	0.763	0.755
	3.0	0.700	0.699	0.689	0.678
50	2.0	0.844	0.837	0.809	0.771
	2.5	0.771	0.762	0.715	0.654
	3.0	0.697	0.687	0.608	0.497
100	2.0	0.834	0.802	0.646	0.475
	2.5	0.759	0.704	0.427	0.157
	3.0	0.683	0.586	0.118	-

6. Conclusions

This study investigated the residual shear resistances after one-directional repeated loads on the Y-type perfobond rib shear connectors. The development procedure for a design formula was proposed to provide a design residual shear strength according to the properly selected target reliability level. The conclusions are as follows:

(1) The design residual shear resistance formula under repeated loads was proposed with a resistance (reduction) factor, which can be selected depending on the target reliability level under the repeated load environments. The various reduction factors were provided for the range of target reliability index from 2.0 to 3.0. The proposed procedure can be applied to the other Y-type perfobond rib shear connectors with different design variables and repeated load intensities such as different Y-rib sizes, rebars, concrete strengths, etc.

(2) The residual shear strength of Y-type perfobond rib shear connectors was found to decrease linearly with cumulated energy dissipation due to the repeated loads. The decreasing rate was evaluated to be quite stable with 2×10^{-5}. The nominal residual shear strength can be estimated from the residual shear strength factor and the nominal shear strength. The residual shear strength factor was estimated by empirical data from the monotonic loading tests on the various specimens that have experienced various repeated loads.

(3) It was found that the energy dissipation per each repeated load converges after 5–10 repetitions when the load intensity is up to 65% of the ultimate shear strength. However, the repeated load intensities over 65% of the ultimate shear strength generate scattered energy dissipations. It was also found that the residual slip increment due to repeated load does not become stable when the repeated load intensity exceeds 55% of the ultimate shear resistance.

(4) From the load–strain relationships on the Y-ribs and rebars, it was found that Y-ribs contribute mainly to the shear resistance when the load is below 55% of the ultimate shear strength.

(5) The residual ductility of Y-type perfobond rib shear connector remains intact after the repeated loads, given that the intensity of the repeated loads does not exceed 65% of the ultimate shear strength.

Author Contributions: Conceptualization, methodology, writing—review, S.-H.K.; formal analysis, O.H., S.Y. and T.B.; specimen and experiment, O.H., S.Y. and T.B.; writing—draft preparation, O.H.; All authors have read and agreed to the published version of the manuscript.

Funding: This work was supported by the Korea Institute of Energy Technology Evaluation and Planning (KETEP) and the Ministry of Trade, Industry & Energy (MOTIE) of the Republic of Korea (No. 20194030202460).

Institutional Review Board Statement: Not applicable.

Informed Consent Statement: Not applicable.

Data Availability Statement: Not applicable.

Conflicts of Interest: The authors declare no conflict of interest.

Appendix A. Energy Dissipation Models under Repeated Loads

Table A1. Average energy dissipation per cycle (five cycles of 785 kN) (unit = kN·mm).

Cycle	1	2	3	4 *	5 *
Specimens	12	→	→	→	→
Averaged dissipated energy	65.06	35.03	26.97	25.79	23.56
Min.	44.18	14.66	10.67	12.58	7.12
Max.	99.84	61.26	49.78	49.76	53.54

* Selected sample space.

Table A2. Average energy dissipation per cycle (five cycles of 1010 kN after 5-785 kN cycles) (unit = kN·mm).

Cycle	1	2	3	4 *	5 *
Specimens	12	→	→	→	→
Averaged dissipated energy	71.66	55.45	48.97	45.02	45.86
Min.	50.95	33.44	24.54	11.52	21.47
Max.	100.57	85.76	85.81	89.89	88.44

* Selected sample space.

Table A3. Average energy dissipation per cycle (five cycles of 1235 kN after 5-785 kN and 5-1010 kN cycles) (unit = kN·mm).

Cycle	1	2	3	4	5	6	7	8	9	10 *
Specimens	12	→	→	→	→	6	→	→	→	→
Averaged dissipated energy	121.59	92.13	86.56	81.27	81.54	67.32	67.85	64.99	68.29	61.39
Min.	82.30	46.50	55.20	41.41	47.80	35.34	45.77	40.16	40.81	30.59
Max.	118.37	74.06	79.28	74.42	71.24	70.43	74.29	68.40	67.71	70.30
Cycle	11 *	12 *	13 *	14	15	16	17	18	19	20
Specimens	→	→	→	→	→	→	→	→	→	→
Averaged dissipated energy	58.90	62.69	64.47	62.99	61.50	63.86	60.47	59.88	60.68	60.38
Min.	28.17	41.12	37.38	41.62	28.12	40.25	40.37	40.68	39.67	38.57
Max.	71.95	69.69	73.44	74.56	75.35	69.83	68.15	65.86	63.19	67.78
Cycle	21	22	23	24	25	26	27	28	29	30
Specimens	→	→	→	→	→	3	→	→	→	→
Averaged dissipated energy	59.07	60.22	57.86	58.44	54.09	56.54	57.83	53.09	45.81	50.61
Min.	37.52	34.79	29.17	33.56	22.93	43.13	47.33	43.60	29.38	30.03
Max.	64.76	69.54	68.53	70.69	67.87	74.69	74.84	68.19	62.99	72.32
Cycle	31	32	33	34	35	36	37	38	39	40
Specimens	→	→	→	→	→	→	→	→	→	→
Averaged dissipated energy	44.32	49.99	44.51	53.90	53.97	45.70	48.56	51.56	50.98	52.86
Min.	25.57	34.68	19.91	44.89	46.70	20.14	37.73	46.43	41.40	37.68
Max.	61.89	66.28	69.36	67.75	67.08	66.26	63.56	60.62	66.37	72.50
Cycle	41	42	43	44	45	46	47	48	49	50
Specimens	→	→	→	→	→	→	→	→	→	→
Averaged dissipated energy	54.27	53.46	51.48	49.30	53.48	53.52	50.83	50.44	48.90	56.32
Min.	44.91	45.76	38.20	36.77	45.93	45.96	38.61	36.27	33.28	48.01
Max.	67.53	68.69	70.08	67.60	67.70	64.42	70.80	68.94	67.83	71.79

* Selected sample space.

Table A4. Averaged energy dissipation per cycle (five cycles of 1460 kN after 5-785 kN and 5-1010 kN and 5-1235 kN cycles) (unit = kN·mm).

Cycle	1	2	3	4	5	6	7	8	9 *	10 *
Specimens	5	→	→	→	→	4	→	→	→	→
Averaged dissipated energy	258.27	220.60	175.35	168.77	154.27	171.79	162.19	157.32	155.22	155.58
Min.	227.67	191.44	153.79	141.81	127.38	130.89	127.33	126.33	124.03	114.88
Max.	338.78	241.86	207.18	215.91	209.57	216.71	211.12	217.01	203.64	203.03
Cycle	11 *	12 *	13 *	14 *	15 *					
Specimens	3	→	→	→	→					
Averaged dissipated energy	151.77	154.45	153.60	159.18	153.97					
Min.	120.83	116.19	120.48	129.26	124.16					
Max.	207.66	208.04	207.15	207.48	202.40					

* Selected sample space.

References

1. Bursi, O.S.; Gramola, G. Behaviour of headed stud shear connectors under low cycle high amplitude displacements. *Mater. Struct.* **1999**, *32*, 290–297. [CrossRef]
2. Zandonini, R.; Bursi, O.S. Cyclic behavior of headed stud shear connectors. *Compos. Constr. Steel Concr. IV* **2002**, 470–482. [CrossRef]
3. Nakajima, A.; Saiki, I.; Kokai, M.; Doi, K.; Takabayashi, Y.; Ooe, H. Cyclic shear force–slip behavior of studs under alternating and pulsating load condition. *Eng. Struct.* **2003**, *25*, 537–545. [CrossRef]
4. Maleki, S.; Bagheri, S. Behavior of channel shear connectors, Part I: Experimental study. *J. Constr. Steel Res.* **2008**, *64*, 1333–1340. [CrossRef]
5. Shariati, A.; Shariati, M.; Sulong, N.R.; Suhatril, M.; Khanouki, M.A.; Mahoutian, M. Experimental assessment of angle shear connectors under monotonic and fully reversed cyclic load in high strength concrete. *Constr. Build. Mater.* **2014**, *52*, 276–283. [CrossRef]
6. Shariati, M.; Shariati, A.; Sulong, N.R.; Suhatril, M.; Khanouki, M.A. Fatigue energy dissipation and failure analysis of angle shear connectors embedded in high strength concrete. *Eng. Fail. Anlys.* **2014**, *41*, 124–134. [CrossRef]
7. Shariati, M.; Sulong, N.R.; Suhatril, M.; Shariati, A.; Khanouki, M.A.; Sinaei, H. Comparison of behaviour between channel and angle shear connectors under monotonic and fully reversed cyclic load. *Constr. Build. Mater.* **2013**, *38*, 582–593. [CrossRef]
8. Kim, K.S.; Han, O.; Choi, J.; Kim, S.H. Hysteretic performance of stubby Y-type perfobond rib shear connectors depending on transverse rebar. *Constr. Build. Mater.* **2019**, *200*, 64–79. [CrossRef]
9. Kim, D.Y.; Gombosuren, M.; Han, O.; Kim, S.H. Hysteretic model of Y-type perfobond rib connectors with large number of ribs. *J. Constr. Steel Res.* **2020**, *166*, 105818. [CrossRef]
10. Kim, K.S.; Han, O.; Heo, W.H.; Kim, S.H. Behavior of Y-type perfobond rib shear connection under different cyclic loading conditions. *Structure* **2020**, *26*, 562–571. [CrossRef]
11. Kim, S.H.; Kim, K.S.; Park, S.; Jung, C.Y.; Choi, J.G. Comparison of hysteretic performance of stubby Y-type perfobond rib and stud shear connectors. *Eng. Struct.* **2017**, *147*, 114–124. [CrossRef]
12. Suzuki, A.; Kimura, Y. Cyclic behavior of component model of composite beam subjected to fully reversed cyclic loading. *J. Struct Eng.* **2019**, *145*, 04019015. [CrossRef]
13. Suzuki, A.; Abe, K.; Suzuki, K.; Kimura, Y. Cyclic Behavior of Perfobond-Shear Connectors Subjected to Fully Reversed Cyclic Loading. *J. Struct. Eng.* **2021**, *147*, 04020355. [CrossRef]
14. Kisaku, T.; Fujiyama, C. Modeling the cyclic response of perfobond-rib shear connectors. *Pro. Eng.* **2017**, *171*, 1317–1324. [CrossRef]
15. Wang, Y.H.; Yu, J.; Liu, J.; Chen, Y.F. Experimental and Numerical Analysis of Steel-Block Shear Connectors in Assembled Monolithic Steel–Concrete Composite Beams. *J. Bridge Eng.* **2019**, *24*, 04019024. [CrossRef]
16. Wang, X.; Liu, Y.; Liu, Y. Experimental study on shear behavior of notched long-hole perfobond connectors. *Adv. Struct. Eng.* **2019**, *22*, 202–213. [CrossRef]
17. Wang, Y.H.; Yu, J.; Liu, J.P.; Chen, Y.F. Shear behavior of shear stud groups in precast concrete decks. *Eng Struct.* **2019**, *187*, 73–84. [CrossRef]
18. Ramesh, D.; Sadhana, J.; Ganesh, B.; Gunasekaran, U. Enhancement of shear connectors for steel-concrete composite structures. *J. Struct. Eng.* **2015**, *42*, 363–369.
19. Kim, S.H.; Choi, K.T.; Park, S.J.; Park, S.M.; Jung, C.Y. Experimental shear resistance evaluation of Y-type perfobond rib shear connector. *J. Constr. Steel Res.* **2013**, *82*, 1–18. [CrossRef]
20. Kim, S.H.; Park, S.J.; Heo, W.H.; Jung, C.Y. Shear resistance characteristic and ductility of Y-type perfobond rib shear connector. *Steel Compos. Struct.* **2015**, *18*, 497–517. [CrossRef]
21. Kim, S.H.; Kim, K.S.; Han, O.; Park, J.S. Influence of transverse rebar on shear behavior of Y-type perfobond rib shear connection. *Constr. Build. Mat.* **2018**, *180*, 254–264. [CrossRef]

22. Kim, S.H.; Han, O.; Kim, K.S.; Park, J.S. Experimental behavior of double-row Y-type perfobond rib shear connectors. *J. Constr. Steel Res.* **2018**, *150*, 221–229. [CrossRef]
23. *Korean Standard D3503: Rolled Steels for General Structure*; Korean Agency for Technology and Standards: Chungcheongbuk-do, Korea, 2018.
24. Eurocode 4–1994. *Design of Composite Steel and Concrete Structures, Part. 1.1: General Rules and Rules for Buildings, EN1994-1-1*; European Committee for Standardization: Brussels, Belgium, 2004.
25. Ang, A.H.-S.; Tang, W.H. *Probability Concepts in Engineering*; Wiley: Hoboken, NJ, USA, 2007; Volume 1.
26. Kim, S.H.; Batbold, T.; Shah, S.H.A.; Yoon, S.; Han, O. Development of shear resistance formula for the Y-type perfobond rib shear connector considering probabilistic characteristics. *Appl. Sci.* **2021**, *11*, 3877. [CrossRef]